FRONT MATTER

Title

- Full title: **HSPB8 regulates CTP synthase filaments to couple nucleotide metabolism and autophagy in tumors**

Authors

Wei-Cheng Lin[1†], Chun-Yen Wang[2†], Kuang-Jing Huang[3], Archan Chakraborty[2,7], Yu-Tsun Lin[1], Ya-Ju Hsieh[1], Kun-Yi Chien[1,2], Po-Yuan Ke[2,3], Wei-Han Huang[2], Chih-Yun Cheng[4], Ian Yi-Feng Chang[1], Hsiang-Yu Tang[5], Cheng-Hung Yang[5], Mei-Ling Cheng[4,5], Ying-Chih Chang[8,9,10,11], Chau-Ting Yeh[6], Chien-Kuo Lee[12], Jau-Song Yu[1,2], Yu-Sun Chang[1], Jörg Großhans[13], and Li-Mei Pai[1,2,3,6 *]

Affiliations

[1]Molecular Medicine Research Center, College of Medicine,
[2]Graduate Institute of Biomedical Sciences, College of Medicine,
[3]Department of Biochemistry and Molecular Biology, College of Medicine,
[4]Department of Biomedical Sciences, College of Medicine,
[5]Metabolomics Core Laboratory, Healthy Aging Research Center,
Chang Gung University, Taoyuan 33302, Taiwan.
[6]Liver Research Center, Chang Gung Memorial Hospital, Linkou, Taiwan.
[7]Pharmacology and Cancer Biology, Duke University, NC 27705, USA.
[8]AcroCyte Therapeutics, New Taipei City, Taiwan.
[9]Department of Chemical Engineering, Stanford University, Stanford, CA, 94305, USA.
[10]Developmental Biology and Regenerative Medicine Center, National Taiwan University, Taipei 10672, Taiwan.
[11]Genomics Research Center, Academia Sinica, Taipei, Taiwan.
[12]Graduate Institute of Immunology, National Taiwan University College of Medicine, Taipei 100233, Taiwan.
[13]Department of Biology, Philipps University Marburg, Germany.
[†]co-first author
[*]Corresponding author Li-Mei Pai, pai@mail.cgu.edu.tw.

Competing interests:

All other authors declare they have no competing interests.

Abstract

Metabolic adaptation and proteostasis are essential for tumor survival under nutrient stress, yet how these processes are mechanistically integrated remains unclear. Here, we identify CTP synthase (CTPS) filament dynamics as a regulatory nexus linking nucleotide metabolism to autophagic flux. Under glutamine deprivation—a hallmark of poorly vascularized solid tumors—CTPS undergoes polymerization into filamentous assemblies that exhibit reduced enzymatic activity. We demonstrate that filament formation is driven by intracellular asparagine availability and stabilized by the accumulation of misfolded proteins. Using APEX2-based proximity labeling and proteomics, we identify the small heat shock protein HSPB8 as a filament-associated regulator. HSPB8, acting within the chaperone-assisted selective autophagy (CASA) pathway, antagonizes CTPS polymerization by promoting clearance of misfolded proteins, thereby restoring soluble, catalytically active CTPS. Filament disassembly increases CTP production and enhances synthesis of autophagy-related phospholipids, including phosphatidylinositol and phosphatidylethanolamine, resulting in accelerated autophagic flux. Cells expressing filament-deficient CTPS mutants display elevated autophagosome formation and increased LC3-II accumulation upon lysosomal blockade, confirming enhanced flux. In vivo, disruption of CTPS filament assembly impairs xenograft tumor growth and is associated with excessive autophagy. Analysis of TCGA datasets further reveals that high CTPS and low HSPB8 expression correlate with poor patient survival across multiple cancers. Collectively, our findings establish CTPS filament dynamics as a proteostasis-sensitive metabolic switch that coordinates nucleotide biosynthesis with autophagy, revealing a previously unrecognized vulnerability in tumors adapting to nutrient limitation.

MAIN TEXT

Introduction

Adapting to chronic nutrient scarcity is a fundamental challenge for malignant progression. In solid tumors, poor vascularization leads to profound glutamine deprivation, forcing cancer cells to develop sophisticated survival strategies (*1*). To maintain amino acid homeostasis, cells utilize a coordinated network of membrane transport, de novo biosynthesis, and proteostasis—the balance between protein synthesis and autophagic breakdown. Among these adaptive responses, cells increasingly rely on asparagine (Asn) to maintain proliferation under glutamine-depleted conditions (*2-4*). Consequently, asparaginase treatment—which depletes extracellular and intracellular asparagine—is a key therapeutic strategy (*5, 6*). However, the efficacy of this treatment is often limited by adaptive cellular responses, including the induction of autophagy (*7-9*).

Emerging evidence suggests that cellular metabolism is regulated through the dynamic compartmentalization of enzymes into membrane-less organelles or biomolecular condensates. Cytidine triphosphate synthase (CTPS), the rate-limiting enzyme in de novo pyrimidine synthesis, is a prominent example of this phenomenon. CTPS catalyzes the ATP-dependent

conversion of UTP to CTP using glutamine as a nitrogen donor. Under glutamine-deprived conditions, mammalian CTPS undergoes a phase transition to form higher-order polymers and filament bundles, facilitated by specific residues in the linker (R294) and glutaminase (H355) domains (*10, 11*). Furthermore, we have previously shown that the amino acid, histidine can trigger these filamentous structures to assemble along with cytokeratin networks and allow rapid cell growth after stress relief (*12, 13*). While these filaments are known to respond to nutrient cues, the molecular machinery that coordinates their assembly with broader cellular survival programs remains poorly defined.

The maintenance of proteostasis is primarily overseen by molecular chaperones, among which the small heat shock protein B8 (HSPB8) plays a specialized role. Unlike general chaperones, HSPB8 specifically recognizes unfolded peptides and defective ribosomal products (DRiPs), targeting them for degradation via the chaperone-assisted selective autophagy (CASA) complex (*14-16*). By forming a functional unit with the co-chaperone BAG3 and the scaffold protein HSP70, HSPB8 has been shown to actively promote autophagic flux to clear proteotoxic aggregates (*17-19*). While HSPB8 is well-characterized in the context of neurodegenerative protein aggregation, its involvement in regulating the structural dynamics of metabolic enzymes has not been explored. Given that metabolic stress often coincides with proteostatic imbalance, HSPB8 emerges as a potential link between the cellular protein quality control machinery and the adaptive compartmentalization of enzymes like CTPS.

In this study, we identify the availability of asparagine as a key environmental factor governing CTPS filament dynamics. Through proteomic screening, we discovered that HSPB8 serves as a critical metabolic rheostat that antagonizes CTPS polymerization. We demonstrate that filament assembly is driven by the accumulation of unfolded peptides, which act as structural scaffolds for filament bundling. Our results reveal that the HSPB8-mediated disassembly of CTPS filaments is a requisite step for activating autophagic flux under nutrient stress. By releasing soluble, active CTPS, cells increase CTP production to fuel the phospholipid biosynthesis required for autophagosome membrane expansion. Crucially, we show that disrupting this balance to reduce CTPS filament formation leads to significantly impaired tumor growth, identifying the HSPB8-CTPS-autophagy axis as a vital survival response. These findings define a therapeutic vulnerability in cancers with high CTPS expression and provide a new perspective on how cells coordinate their physical and chemical states to survive starvation.

Results

CTPS filament assembly is essential for xenograft tumor progression

Given that CTPS filaments have been identified in clinical tumor specimens (*20*), we hypothesized that these macromolecular structures serve a functional role in oncogenesis. To investigate whether CTPS polymerization regulates tumor growth *in vivo*, we performed xenograft experiments using HCT116 cells expressing either wild-type (WT) CTPS or the filament-deficient H355A mutant (Fig. 1A-B). The filament-deficient H355A mutant cells

exhibited a significant reduction in tumor volume compared to WT controls (Fig. 1C-E). Notably, these phenotypic differences occurred in the absence of systemic toxicity, as indicated by stable murine body weights across cohorts (Fig. 1F).

To further elucidate the mechanisms driving this growth disparity, we characterized the proliferative capacity of these cells under varying environmental conditions. Under glutamine deprivation in three-dimensional (3D) culture (Gln(-)S(+)), HCT116 cells showed negligible growth. However, in nutrient-replete conditions (Gln(+)S(+)), the H355A mutant displayed significantly impaired proliferation specifically in suspension sphere assays (Fig. S1B). This contrast is striking given that the mutant and WT cells exhibited indistinguishable growth rates in standard two-dimensional (2D) monolayer cultures (Fig. S1A). Collectively, these data suggest that CTPS filament assembly is not merely a cellular feature but a critical regulator of 3D proliferative capacity and *in vivo* tumor formation.

Asparaginase inhibits CTP synthase polymerization by depleting intracellular asparagine pools

Asparagine (Asn) is a known survival factor during glutamine deprivation (*3*). Consistent with this role, we observed that CTP synthase (CTPS) filament formation under glutamine-deprived conditions was inhibited by asparaginase (ASNase) treatment (Fig. 2, A to F) without altering total CTPS protein levels (Fig. 2G). Conversely, exogenous Asn supplementation promoted CTPS polymerization (Fig. 2, C to F). To further define the specificity of this effect, we screened the remaining non-essential amino acids—alanine, asparagine, aspartate, and proline—for their capacity to induce filamentation. Our results confirm that Asn induces CTPS filaments, comparable to the histidine positive control (Fig. S2A). Supporting this, the combination of Asn and ASNase treatment nearly abolished CTPS filamentation in EBSS, a conditional medium without any amino acid supplementation (Fig. S2B).

Given that Asn is absent from DMEM, we hypothesized that serum serves as the primary source of Asn for filament assembly. Quantitative metabolic analysis revealed that Asn levels increase during glutamine deprivation relative to standard DMEM but are depleted upon serum withdrawal or ASNase treatment (Fig. S2C). Although extracellular nutrients can be scavenged via macropinocytosis to support proliferation under nutrient stress (*21*), Asn can also be synthesized de novo by asparagine synthetase (ASNS). However, ASNS knockdown did not affect CTPS filamentation (Fig. S2, D and E), likely due to substrate limitations of glutamine required for ASNS enzymatic activity (*22*). Collectively, these data demonstrate that intracellular Asn levels regulate CTPS filament dynamics, suggesting a metabolic adaptation where cells modulate amino acid homeostasis to confer nutrition stress during glutamine deprivation.

Identification of CTPS-associated proteins via APEX2 proximity labeling

To elucidate the mechanisms governing CTP synthase (CTPS) filament dynamics, we employed APEX2-based proximity labeling to identify protein interactors in situ (*23*). Although CTPS filaments assemble during nutrient starvation, their structural integrity is highly sensitive to cell lysis, which typically precludes traditional biochemical purification.

We therefore generated HEp-2 cell lines stably expressing a CTPS-APEX2 fusion protein to biotinylate proximal proteins in living cells (*13*). To ensure high specificity for filament-associated partners, we utilized two negative controls representing a non-filamentous state: glutamine-induced disassembly and a polymerization-deficient R294D mutant (*12, 24*) (Fig. 3A). Western blot analysis confirmed that both endogenous CTPS and exogenous CTPS-APEX2 levels were markedly elevated under glutamine deprivation, consistent with reports that filamentation protects CTPS from proteasomal degradation (*12*). Furthermore, the enrichment of the known filament-associated protein IMPDH2 (*25*) in the CTPS-APEX2 pull-down validated the spatial accuracy and efficacy of our proximity labeling system (Fig. 3B).

Discovery of HSPB8 as a CTPS filament-associated protein regulated by asparaginase

To define the CTPS filament proteome with high stringency, we integrated data from two independent proteomics experiments and applied a fold-change cutoff based on IMPDH2 enrichment (Fig. S3, A to C). This filtering strategy yielded 184 overlapping proteins significantly enriched in pathways involving de novo purine biosynthesis and protein ubiquitination (Fig. 3C). IMPDH2 and PFAS in the purine de novo biosynthesis category have been demonstrated to form distinct compartments, filament, and purinosome, respectively (*26, 27*). Notably, the identification of multiple heat shock proteins (e.g., HSPA4, HSPB8, HSPH1) and deubiquitinating enzymes in the protein ubiquitination category suggests that protein quality control (PQC) machinery localizes proximally to CTPS filaments during metabolic stress. Given that asparagine (Asn) is a key effector of ATF4-mediated amino acid homeostasis, we hypothesized that Asn availability modulates this PQC-filament association (*4, 28*). Quantitative proteomics and subsequent western blotting validation revealed that the small heat shock protein HSPB8 is downregulated during glutamine deprivation but specifically upregulated upon ASNase treatment (Fig. 3, D and E). We further confirmed the physical proximity between CTPS and HSPB8 through a proximity ligation assay (PLA) (Fig. S3D), establishing HSPB8 as a putative regulator of CTPS filament dynamics under glutamine-deprived stress.

HSPB8 regulates the compartmentalization of CTPS filaments

HSPB8, a member of the small heat shock protein (sHSP) family, acts in concert with BAG3—and often within the chaperone-assisted selective autophagy (CASA) complex alongside HSP70 and E3 ligases—to facilitate the clearance of misfolded or aggregation-prone protein. Given its established role in maintaining proteostasis, we hypothesized that the ASNase-induced upregulation of HSPB8 promotes the disassembly of CTPS filaments. To test this, we performed loss- and gain-of-function assays to evaluate the requirement of HSPB8 for CTPS filament dynamics. Under glutamine-deprived conditions, HSPB8 knockdown significantly enhanced CTPS filament assembly compared to control groups (Fig. 4, A and B). Conversely, we observed that the restoration of glutamine, which typically triggers filament disassembly, was less effective in the absence of HSPB8, resulting in persistent filament structures (Fig. 4, A and B).

In contrast to the knockdown phenotypes, overexpression of HSPB8 markedly reduced

the prevalence of CTPS filaments assembly, suggesting that HSPB8 facilitates the release of CTPS from filamentous compartments into the cytosol (Fig. 4, C and D). Crucially, we found that HSPB8 depletion was sufficient to restore CTPS filament assembly even in the presence of ASNase treatment, which normally prevents filament assembly (Fig. 4, E and F). Collectively, these results demonstrate that ASNase disassembles CTPS filaments by upregulating HSPB8, identifying this chaperone as a key molecular rheostat for CTPS assembly during glutamine-deprived stress.

Clinical significance of the HSPB8-CTPS axis in cancer prognosis

Although CTPS expression and enzymatic activity have been established as drivers of malignant progression (*29*), the clinical relevance of its regulatory partnership with HSPB8 remains poorly defined. To investigate this, we analyzed expression profiles across several cancer types using The Cancer Genome Atlas (TCGA) database. Our analysis revealed that CTPS expression is significantly elevated, while HSPB8 expression is markedly reduced, in multiple malignancies compared to adjacent normal tissues, including breast invasive carcinoma (BRCA), colon adenocarcinoma (COAD), head and neck squamous cell carcinoma (HNSCC), lung adenocarcinoma (LUAD), lung squamous cell carcinoma (LUSC), rectum adenocarcinoma (READ), stomach adenocarcinoma (STAD), and thyroid carcinoma (THCA) (Fig. S4, A and B).

To evaluate the prognostic impact of this inverse correlation, we performed Kaplan-Meier survival analysis. We found that patients with high CTPS expression combined with low HSPB8 expression exhibited significantly poorer survival outcomes in adrenocortical carcinoma (ACC), pancreatic adenocarcinoma (PAAD), sarcoma (SARC), and pheochromocytoma and paraganglioma (PCPG) (Fig. 4 G and S4 C). These clinical data suggest that an environment characterized by low HSPB8 levels—which we have shown promotes CTPS filament assembly—may drive tumor progression and serves as a negative prognostic signature in several human cancers.

Glutamine deprivation-induced misfolded protein accumulation drive CTPS filamentation

Since HSPB8 targets misfolded proteins for autophagic clearance and our proteomic data identified protein quality control (PQC) machinery in the CTPS interactome (Fig. 3C), we hypothesized that the accumulation of unfolded proteins modulates CTPS filament dynamics. Proximity ligation assays (PLA) confirmed that the CTPS-HSPB8 association is spatially restricted to CTPS filaments (Fig. S5A). Furthermore, we observed an increased association between HSPB8 and its co-chaperone BAG3 under glutamine deprivation (Fig. S5B), suggesting an active role for the HSPB8-BAG3 complex in managing protein misfolding during metabolic stress.

To evaluate the direct impact of proteotoxic stress on CTPS polymerization, we treated cells with puromycin to induce the premature termination of translation and the subsequent generation of defective ribosomal products (DRiPs) (*30*). Under glutamine-deprived conditions, puromycin treatment resulted in the formation of significantly thicker CTPS

filaments compared to untreated controls (Fig. 5, A and B). The proximity biotin-labeling with streptavidin pull-down experiment revealed that puromycylated polypeptides are enriched in the immediate vicinity of CTPS filaments (Fig. 5C), implying that local proteotoxic stress exerts a stabilizing effect on filament dynamics.

Consistent with its role in protein clearance, the knockdown of HSPB8 led to a marked accumulation of puromycylated polypeptides (Fig. 5D and Fig. S5C). Conversely, the intensity of these misfolded protein signals significantly declined upon ASNase treatment (Fig. 5E). Taken together, these findings demonstrate that HSPB8 regulates CTPS filament dynamics by modulating the local concentration of unfolded proteins, positioning the filament as a metabolic structure sensitive to cellular proteostasis.

CTPS filament disassembly promotes autophagic flux under glutamine-deprived stress

Autophagy is a critical survival mechanism during asparaginase-induced cytotoxicity. Given that CTP is a requisite substrate for the de novo synthesis of choline phospholipids—catalyzed by PCYT1A (phosphate cytidylyltransferase 1, choline, alpha) to replenish autophagosome membranes (*31*)—we investigated whether the disassembly of CTPS filaments enhances autophagic capacity. We previously established that non-filamentous CTPS possesses higher enzymatic activity than its polymerized counterpart. Consistent with this, our in vivo enzymatic assays, measuring the $^{13}C^{15}N$-CTP to $^{13}C^{15}N$-UTP ratio, demonstrated that filament-null mutants (R294D and H355A) exhibit significantly higher catalytic activity compared to wild-type CTPS (Fig. S6A).

To determine if increased CTPS activity promotes autophagy, we utilized mRFP-GFP-LC3 reporter cell lines to monitor autophagic flux (*32*). Under glutamine deprivation, $CTPS^{R294D}$ or $CTPS^{H355A}$ cells displayed a higher density of mRFP-positive/GFP-negative puncta per cell than $CTPS^{WT}$ cells, indicating an acceleration of autolysosome formation (Fig. 6, A and B; Fig. S6, B and C). Transmission electron microscopy (TEM) further confirmed a marked accumulation of both early (AVi) and late (AVd) autophagic vacuoles in filament-null mutants, whereas wild-type cells exhibited significantly fewer structures (Fig. 6, C and D; Fig. S6, D and E). To distinguish between increased induction and blocked degradation, we treated cells with Bafilomycin A1 (BafA1) to inhibit lysosomal fusion. Under BafA1 treatment, filament-null cells accumulated significantly higher levels of LC3-II compared to wild-type controls, confirming that CTPS disassembly actively enhances autophagic flux (Fig. 6, E and F). Collectively, these findings suggest that the metabolic regulation of CTPS filament dynamics modulates autophagic activity.

HSPB8 promotes autophagy by antagonizing CTPS filament assembly

Building on findings identifying the chaperone HSPB8 as a negative regulator of CTP synthase (CTPS) polymerization, we investigated the role of CTPS filament dynamics within the HSPB8-autophagy axis during glutamine-deprived nutrient stress. HSPB8, a member of the small heat shock protein family, specifically binds unfolded peptides and has been previously implicated in the induction of autophagy (*33*). To determine if CTPS filament disassembly is a requisite step in this process, we evaluated autophagic flux under glutamine-

and serum-deprived conditions (Gln(-)S(-))In cells expressing wild-type CTPS ($CTPS^{WT}$), overexpression of HSPB8 significantly increased the number of autolysosomes (mRFP-positive/GFP-negative) and total autophagic vesicles compared to vehicle-treated controls (Fig. 7, A, C, and E). In contrast, HSPB8 overexpression failed to further enhance autophagic vesicle accumulation in filament-deficient $CTPS^{H355A}$ cells (Fig. 7, B, D, and E). These results suggest that the pro-autophagic effect of HSPB8 under glutamine deprivation is mediated through the inhibition of CTPS filament assembly, identifying the transition from polymerized to dimeric or tetrameric CTPS as a critical metabolic switch for autophagic activation.

Reduced volume of $CTPS^{H355A}$ tumors correlates with excessive autophagy activity

Given that $CTPS^{H355A}$ cells exhibit both impaired filament assembly and elevated autophagy in vitro, we sought to determine if this relationship holds true in a physiological tumor model. We analyzed the widely-used autophagy marker LC3B in $CTPS^{WT}$ - and $CTPS^{H355A}$ -derived tumors (from Fig. 1) to understand how defective filament assembly interferes with tumor progression (Fig. S7A). Consistently, the LC3B-II/LC3B-I ratio, a hallmark of autophagic flux, was elevated in $CTPS^{H355A}$ tumors (Fig. S7B). These findings suggest that the anti-tumor effect observed when CTPS filament assembly is disrupted is associated with an induction of excessive autophagic activity.

Phospholipid biosynthesis is upregulated in filament-deficient CTPS mutants

Because CTPS facilitates phospholipid biosynthesis through CTP production, we hypothesized that filament-deficient mutants exhibit elevated autophagy due to an increased supply of membrane building blocks. Given that lipids and lipid-associated proteins are indispensable for autophagosome formation and maturation, we performed liquid chromatography-mass spectrometry (LC-MS) to compare the lipidomic profiles of $CTPS^{WT}$ and $CTPS^{R294D}$ HEp-2 cells. We identified 75 annotated lipids that met the significance criteria of $P < 0.05$, fold change > 1.3, and a Variable Importance in Projection (VIP) score > 1 (Fig. 8A and Fig. S8, A to C). A heatmap of 43 high-confidence lipids which was verified by MS/MS identification revealed a consistent elevation in $CTPS^{R294D}$ cells, correlating with the increased enzymatic activity of the non-filamentous mutant (Fig. 8B). LIPEA pathway analysis indicated a significant enrichment of autophagy-related lipids, specifically phosphatidylethanolamines (PE) and phosphatidylinositols (PI), which were significantly higher in $CTPS^{R294D}$ cells (Fig. 8, C and D). Since PI and PE are essential for autophagosome membrane initiation and expansion, these findings suggest that the metabolic output of disassembled CTPS directly supports the lipid requirements for enhanced autophagic flux.

Discussion

Metabolic enzymes increasingly are recognized for their ability to undergo higher-order compartmentalization in response to physiological stress, yet the functional consequences of these transitions remain poorly understood. Our findings demonstrate that the polymerization of CTP synthase (CTPS) into filamentous structures is a critical regulatory event that dictates tumor growth and metabolic adaptation. By integrating biochemical analysis, 3D cell culture,

and clinical datasets, we show that CTPS filaments serve as a metabolic switch that balances enzyme activity with proteostatic demands (**Fig. 1 and Fig. S1**). Specifically, under glutamine deprivation—a hallmark of the nutrient-poor core of solid tumors (*1*)—the assembly of CTPS filaments suppresses enzymatic activity, thereby modulating phospholipid availability and autophagic flux to influence tumor progression.

A key revelation of this study is the identification of the HSPB8-CTPS filament axis as a novel branch of the cellular protein quality control (PQC) system. Building on our previous evidence that ubiquitination regulates CTPS polymerization (*34, 35*), we identified a suite of PQC-related proteins associated with the filament interactome (**Fig. 3**). The chaperone HSPB8, acting within the HSPB8-BAG3 complex, emerged as a master regulator of these dynamics. Our data suggest that misfolded proteins, or defective ribosomal products (DRiPs), localize to and stabilize CTPS filaments. By modulating the clearance of these proteotoxic species, HSPB8 dictates the architectural state of CTPS. The knockdown of HSPB8 promotes filament bundling, while its overexpression triggers disassembly (**Fig. 4 A-F**). This mirrors the role of the HSPB8-BAG3-HSP70 complex in regulating the phase transition of stress granules, suggesting a universal role for HSPB8 in maintaining the fluidity and dynamics of biomolecular condensates and membrane-less organelles.

The biological significance of this regulation is underscored by our analysis of TCGA datasets, where we observed a pervasive inverse relationship between CTPS and HSPB8 expression across 75% of cancer types (**Fig. S4, A and B**). The "high-CTPS/low-HSPB8" signature—which our model predicts would favor stable filament formation—correlates significantly with reduced patient survival (**Fig. 4 G and S4 C**). This suggests that the stabilization of CTPS filaments may provide a selective advantage in aggressive malignancies, likely by sequestering enzymatic activity until metabolic conditions require its mobilization. Consequently, the molecular machinery governing CTPS assembly represents a promising, yet unexplored, therapeutic vulnerability in cancer.

Mechanistically, we establish that the transition from filamentous to soluble CTPS is a prerequisite for autophagic activation (**Fig. 6 and Fig. S6**). While it is well known that autophagy is essential for surviving starvation, we found that the pro-autophagic effects of HSPB8 are strictly dependent on the filamentous state of CTPS (**Fig. 7**). The disassembly of these structures facilitates CTP production, providing the necessary energy and substrates for phosphatidylcholine biosynthesis, which is required for autophagosome membrane expansion. Our lipidomic profiles confirm that autophagy-essential lipids, such as PI and PE, are upregulated upon filament disassembly (**Fig. 8**). In the context of the tumor microenvironment, the mobilization of CTPS and the resulting surge in autophagy may interfere with tumor growth (**Fig. S7**), as excessive autophagic flux can trigger apoptosis or metabolic exhaustion (*36, 37*).

Finally, our study identifies the structural dynamics of CTPS as a direct downstream target of the cellular PQC response. We propose that the accumulation of unfolded peptides serves as a molecular scaffold that promotes CTPS filament bundling. This process is highly sensitive to the cellular methylation status (*12*), as evidenced by the disassembly of CTPS

filaments upon treatment with the methylation inhibitor Adox (**Fig. S2F**). Under metabolic stress and asparaginase treatment, the upregulation of HSPB8 facilitates the clearance of these filament-associated misfolded proteins (**Fig. 2 and Fig. 3E**). This HSPB8-mediated transition, potentially modulated by methylation-dependent signaling (*38*), ensures that cells can reallocate metabolic resources from a sequestered state into active CTP synthesis to meet the demands of autophagic flux. Collectively, these findings position the CTPS filament as a structural bridge between protein quality control and metabolic homeostasis, revealing that targeting the unfolded protein-HSPB8 axis could disrupt the safeguards enabling cancer cell survival (**Fig. 8E**).

Materials and methods

Cells

Human HEp-2 and HeLa cells were cultured in Dulbecco's Modified Eagle's Medium (Gibco) supplemented with 10% fetal bovine serum. Human HCT116 cells were culture in McCoy's 5A Medium (Sigma). All of cells were maintained at 37°C under 5% CO^2, and passage was done every 3~4 days. Cells were wash with 1X PBS twice before any medium change.

3D spheroid culture

HCT116 cells were seeded in the R^3CE platform (Acrocyte Therapeutics Inc., New Taipei City, Taiwan) and incubated in McCoy's 5A medium (with 10% FBS), and appropriate amount of fresh medium is replenished every 3-4 days. Spheroid images were captured by Nikon Eclipse-TS100 microscope with LeadView-2000AIO camera and the spheroid sizes were quantified by imageJ. The spheroids at day 21 were fixed by 4% formaldehyde for 1 h 30 mins and immunostained with CTPS, followed with image capturing by Leica Stellaris SP8 confocal microscope.

Xenograft mouse

Fresh HCT116 WT-CTPS and H355A-CTPS are suspended in McCoy's 5A (without FBS) with Matrigel (M5A: Matrigel=1:1) and subcutaneously injected into right dorsal flank of NUDE mice (BALB/cAnN.Cg-Foxn1nu/CrlNarl). From tumor start to be seen, tumor volume is calculated by length and width (tumor volume V = ½ (Length × Width2)) twice a week. Until 28 days after injection, mice are sacrificed and tumors are collected for further experiments.

Statistical Analysis

Experiment data are analyzed by Student's t test or Kaplan-Meier analysis. Results includes at least 3 biological repeats show means and standard deviation (SD) values with P-values: *<0.05, **<0.01, ***<0.001, ****<0.0001. Other statistical details are included in figure legends.

References

1. M. Pan *et al.*, Regional glutamine deficiency in tumours promotes dedifferentiation

402 through inhibition of histone demethylation. *Nat Cell Biol* **18**, 1090-1101 (2016).
403 2. A. S. Krall, S. Xu, T. G. Graeber, D. Braas, H. R. Christofk, Asparagine promotes
404 cancer cell proliferation through use as an amino acid exchange factor. *Nat Commun* **7**,
405 11457 (2016).
406 3. N. N. Pavlova *et al.*, As Extracellular Glutamine Levels Decline, Asparagine Becomes
407 an Essential Amino Acid. *Cell Metab* **27**, 428-438 e425 (2018).
408 4. J. Ye *et al.*, The GCN2-ATF4 pathway is critical for tumour cell survival and
409 proliferation in response to nutrient deprivation. *EMBO J* **29**, 2082-2096 (2010).
410 5. P. L. Lorenzi, S. Claerhout, G. B. Mills, J. N. Weinstein, A curated census of
411 autophagy-modulating proteins and small molecules: candidate targets for cancer
412 therapy. *Autophagy* **10**, 1316-1326 (2014).
413 6. L. Willems *et al.*, Inhibiting glutamine uptake represents an attractive new strategy for
414 treating acute myeloid leukemia. *Blood* **122**, 3521-3532 (2013).
415 7. H. Takahashi *et al.*, Autophagy is required for cell survival under L-asparaginase-
416 induced metabolic stress in acute lymphoblastic leukemia cells. *Oncogene* **36**, 4267-
417 4276 (2017).
418 8. P. Song *et al.*, The role of autophagy in asparaginase-induced immune suppression of
419 macrophages. *Cell Death Dis* **8**, e2721 (2017).
420 9. L. Hinze *et al.*, Synthetic Lethality of Wnt Pathway Activation and Asparaginase in
421 Drug-Resistant Acute Leukemias. *Cancer Cell* **35**, 664-676 e667 (2019).
422 10. E. M. Lynch *et al.*, Human CTP synthase filament structure reveals the active enzyme
423 conformation. *Nat Struct Mol Biol* **24**, 507-514 (2017).
424 11. E. M. Lynch, J. M. Kollman, Coupled structural transitions enable highly cooperative
425 regulation of human CTPS2 filaments. *Nat Struct Mol Biol* **27**, 42-48 (2020).
426 12. W. C. Lin *et al.*, Histidine-Dependent Protein Methylation Is Required for
427 Compartmentalization of CTP Synthase. *Cell Rep* **24**, 2733-2745 e2737 (2018).
428 13. A. Chakraborty *et al.*, SNAP29 mediates the assembly of histidine-induced CTP
429 synthase filaments in proximity to the cytokeratin network. *J Cell Sci* **133**, (2020).
430 14. S. Carra, S. J. Seguin, H. Lambert, J. Landry, HspB8 chaperone activity toward
431 poly(Q)-containing proteins depends on its association with Bag3, a stimulator of
432 macroautophagy. *J Biol Chem* **283**, 1437-1444 (2008).
433 15. M. Ganassi *et al.*, A Surveillance Function of the HSPB8-BAG3-HSP70 Chaperone
434 Complex Ensures Stress Granule Integrity and Dynamism. *Mol Cell* **63**, 796-810
435 (2016).
436 16. F. Li, H. Xiao, Z. Hu, F. Zhou, B. Yang, Exploring the multifaceted roles of heat shock
437 protein B8 (HSPB8) in diseases. *Eur J Cell Biol* **97**, 216-229 (2018).
438 17. S. Carra, S. J. Seguin, H. Lambert, J. Landry, HspB8 chaperone activity toward
439 poly(Q)-containing proteins depends on its association with Bag3, a stimulator of
440 macroautophagy. *J Biol Chem* **283**, 1437-1444 (2008).
441 18. V. Arndt *et al.*, Chaperone-assisted selective autophagy is essential for muscle
442 maintenance. *Curr Biol* **20**, 143-148 (2010).

19. R. Cristofani *et al.*, The Regulation of the Small Heat Shock Protein B8 in Misfolding Protein Diseases Causing Motoneuronal and Muscle Cell Death. *Front Neurosci* **13**, 796 (2019).
20. C. C. Chang *et al.*, CTP synthase forms the cytoophidium in human hepatocellular carcinoma. *Exp Cell Res* **361**, 292-299 (2017).
21. C. Commisso *et al.*, Macropinocytosis of protein is an amino acid supply route in Ras-transformed cells. *Nature* **497**, 633-637 (2013).
22. J. Zhang *et al.*, Asparagine plays a critical role in regulating cellular adaptation to glutamine depletion. *Mol Cell* **56**, 205-218 (2014).
23. S. S. Lam *et al.*, Directed evolution of APEX2 for electron microscopy and proximity labeling. *Nat Methods* **12**, 51-54 (2015).
24. S. J. Calise *et al.*, Glutamine deprivation initiates reversible assembly of mammalian rods and rings. *Cell Mol Life Sci* **71**, 2963-2973 (2014).
25. C. C. Chang, G. D. Keppeke, L. Y. Sung, J. L. Liu, Interfilament interaction between IMPDH and CTPS cytoophidia. *FEBS J* **285**, 3753-3768 (2018).
26. Y. Ji, J. Gu, A. M. Makhov, J. D. Griffith, B. S. Mitchell, Regulation of the interaction of inosine monophosphate dehydrogenase with mycophenolic Acid by GTP. *J Biol Chem* **281**, 206-212 (2006).
27. S. An, R. Kumar, E. D. Sheets, S. J. Benkovic, Reversible compartmentalization of de novo purine biosynthetic complexes in living cells. *Science* **320**, 103-106 (2008).
28. A. Nakamura *et al.*, Inhibition of GCN2 sensitizes ASNS-low cancer cells to asparaginase by disrupting the amino acid response. *Proc Natl Acad Sci U S A* **115**, E7776-E7785 (2018).
29. J. C. Williams, H. Kizaki, G. Weber, H. P. Morris, Increased CTP synthetase activity in cancer cells. *Nature* **271**, 71-73 (1978).
30. R. Aviner, The science of puromycin: From studies of ribosome function to applications in biotechnology. *Comput Struct Biotechnol J* **18**, 1074-1083 (2020).
31. G. Andrejeva *et al.*, De novo phosphatidylcholine synthesis is required for autophagosome membrane formation and maintenance during autophagy. *Autophagy* **16**, 1044-1060 (2020).
32. P. Y. Ke, C. W. Chang, Y. C. Hsiao, Baicalein Activates Parkin-Dependent Mitophagy through NDP52 and OPTN. *Cells* **11**, (2022).
33. P. Rusmini *et al.*, The Role of the Heat Shock Protein B8 (HSPB8) in Motoneuron Diseases. *Front Mol Neurosci* **10**, 176 (2017).
34. P. Y. Wang *et al.*, Regulation of CTP Synthase Filament Formation During DNA Endoreplication in Drosophila. *Genetics* **201**, 1511-1523 (2015).
35. L. M. Pai *et al.*, Ubiquitination and filamentous structure of cytidine triphosphate synthase. *Fly (Austin)* **10**, 108-114 (2016).
36. S. Liu, S. Yao, H. Yang, S. Liu, Y. Wang, Autophagy: Regulator of cell death. *Cell Death Dis* **14**, 648 (2023).
37. T. Iba, J. Helms, C. L. Maier, R. Ferrer, J. H. Levy, Autophagy and autophagic cell

death in sepsis: friend or foe? *J Intensive Care* **12**, 41 (2024).
38. H. C. Chang *et al.*, Asparagine deprivation enhances T cell antitumour response in patients via ROS-mediated metabolic and signal adaptations. *Nat Metab* **7**, 918-927 (2025).
39. J. Klawitter, V. Schmitz, J. Klawitter, D. Leibfritz, U. Christians, Development and validation of an assay for the quantification of 11 nucleotides using LC/LC-electrospray ionization-MS. *Anal Biochem* **365**, 230-239 (2007).
40. L. Dai *et al.*, Phosphoinositide-specific phospholipase Cgamma1 inhibition induces autophagy in human colon cancer and hepatocellular carcinoma cells. *Scientific reports* **7**, 13912 (2017).

Acknowledgements

We thank Chang Gung University for the Metabolomics Core Laboratory for assistance with metabolomics analysis, Proteomics Core Laboratory for assistance with proteomic analysis, Microscopy Center for assistance with image capture, TEM and ultramicrotomy, Bioinformatics Core Laboratory for assistance with TCGA database analysis, respectively. We thank the National RNAi Core Facility at Academia Sinica for providing shRNA reagents and related services. We thank Dr. Hui-Kuan Lin, Anna C-C Jang and Tzyy-Choou Wu for their comments on the manuscript. This work was funded by the Ministry of Science and Technology, Taiwan (MOST 111-2311-B-182-001 to L.-M.P. and MOST 108-2321-B-182-004-MY3 to W.-C.L.); the Chang Gung Memorial Hospital (CMRPD1K0591-2, CMRPD1M0171); the “Molecular Medicine Research Center, Chang Gung University” from The Featured Areas Research Center Program within the framework of the Higher Education Sprout Project by the Ministry of Education (MOE) in Taiwan.

Author Contributions

Conceptualization: W.C.L. and L.M.P.
Methodology: K.Y.C., M.L.C., P.Y.K., and C.K.L.
Investigation: W.C.L., C.Y.W., K.J.H., A.C., W.H.H., C.Y.C., Y.T.L., Y.J.H., and H.Y.T.
Validation: A.C.
Visualization: W.C.L., C.Y.W., K.J.H., and A.C.
Data curation: W.C.L., C.Y.W., K.Y.C., Y.T.L., C.H.Y., and M.L.C.
Formal analysis: Y.S.C. and Y.F.C.
Funding acquisition: W.C.L. and L.M.P.
Project administration: L.M.P.
Supervision: Y.S.C. and J.S.Y.
Resources: P.Y.K., C.T.Y., Y.C.C., and C.K.L.
Writing – original draft: W.C.L., C.Y.W., A.C., and L.M.P.
Writing – review & editing: Y.S.C., C.K.L., and J.G.

Data and materials availability:

Under uploading

529 **Figures**

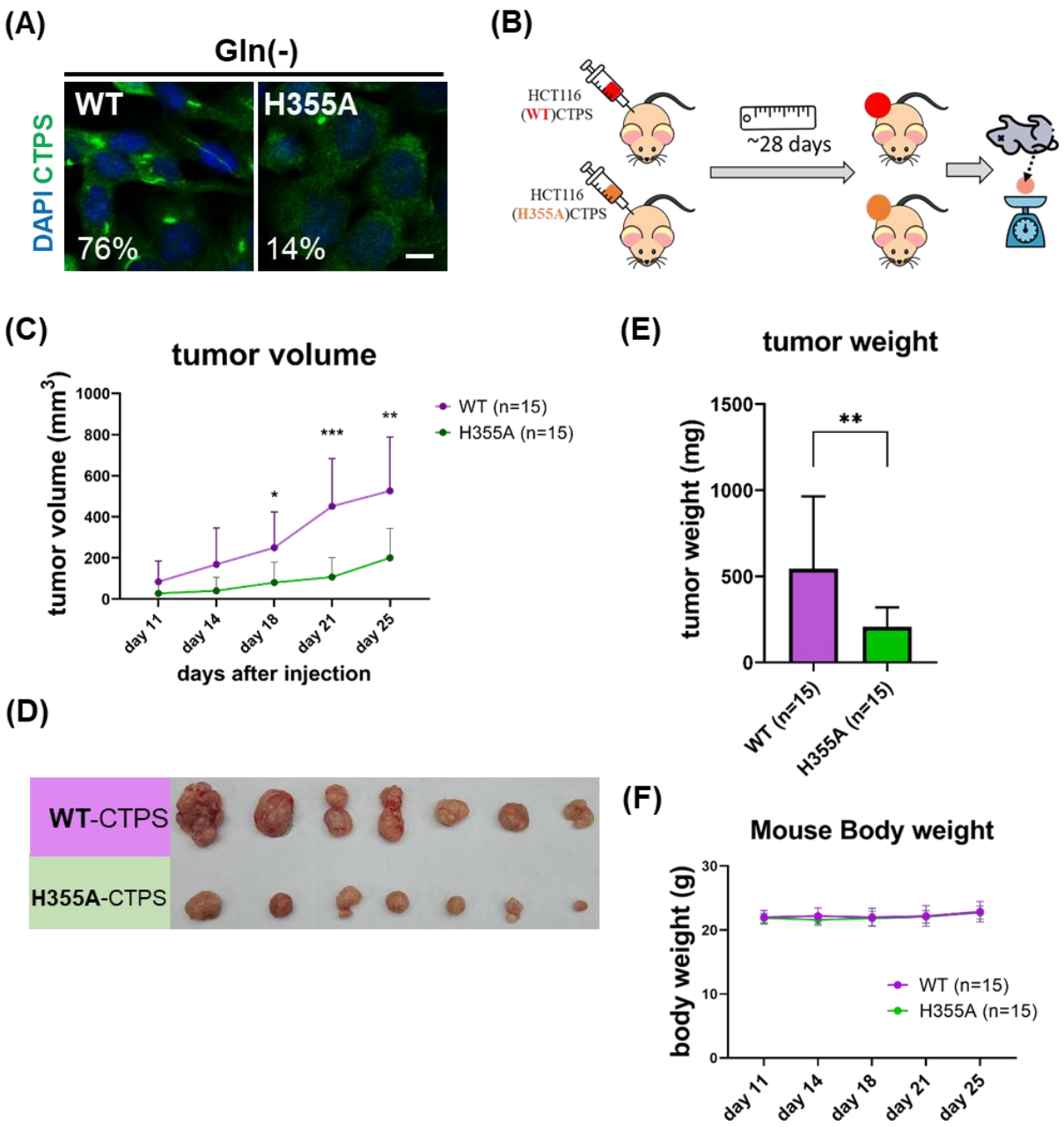

530 **Figure 1. Disrupting CTPS filament assembly impairs HCT116 tumor growth in vivo**
531 **(A)** HCT116 cells stably expressing CTPS^{WT} or CTPS^{H355A} were cultured in Gln-free DMEM
532 for 24 h, and immunostained for CTPS (green); nuclei were counterstained with DAPI (blue).
533 **(B)** Schematic of the xenograft mouse experiment. Thirty mice were used, with 15 injected with
534 HCT116 CTPS^{WT} cells and 15 injected with HCT116 CTPS^{H355A} cells. The experiment was
535 terminated day 28 after injection. **(C)** Tumor volume measured by external caliper throughout
536 the experimental period. **(D)** Representative images of tumors derived from CTPS^{WT} or
537 CTPS^{H355A} cells excised at day 28 after injection; tumor weights are quantified in **(E)**. **(F)** Mouse
538 body weight recorded by scale over the course of the experiment.
539

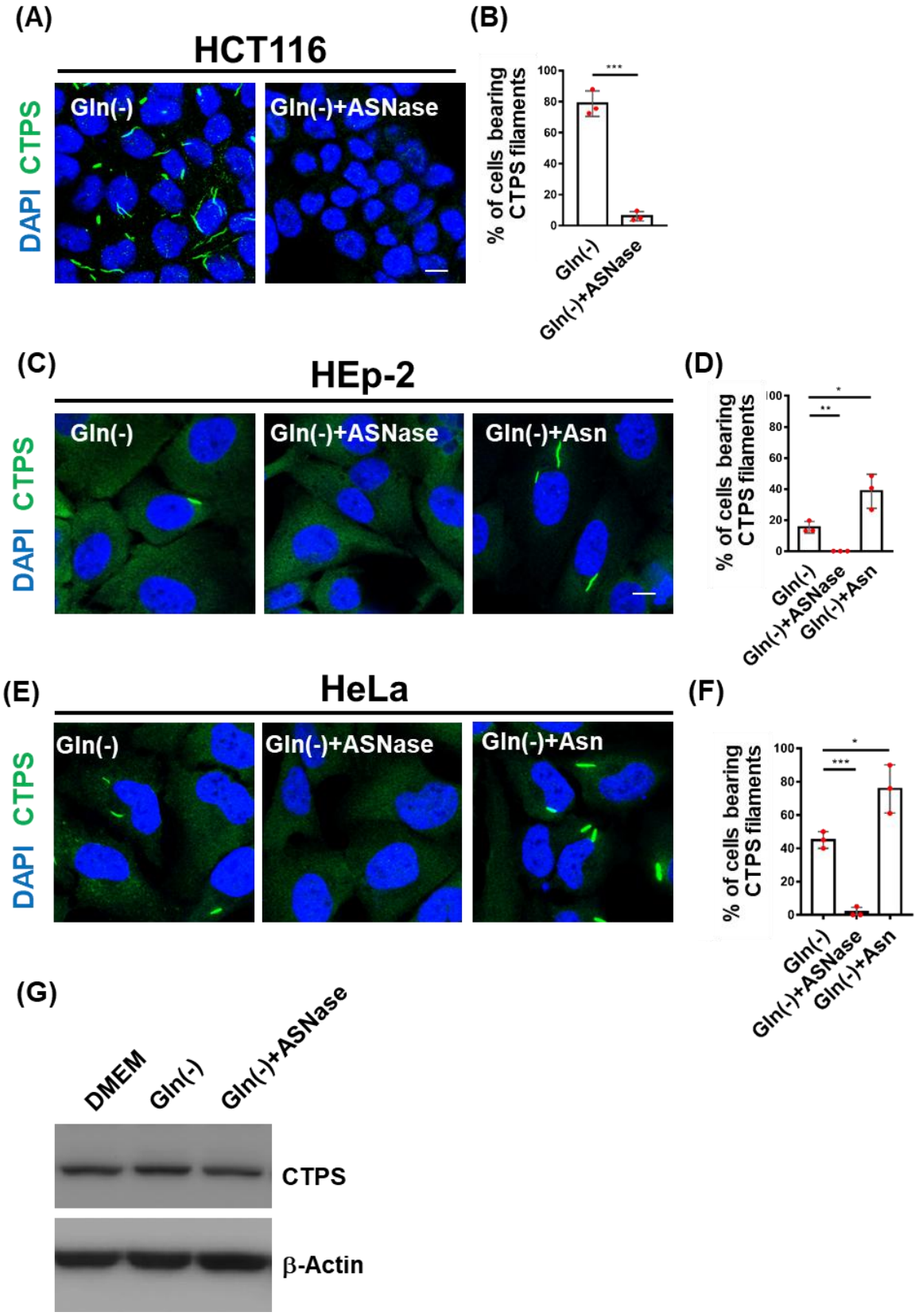

Figure 2. Asparagine availability is essential for CTPS filament assembly under glutamine deprivation

(A, B) HCT116 cells were incubated in Gln-free DMEM or Gln-free DMEM supplemented with ASNase (2U/ml) for 24 h, followed by immunostaining for CTPS (green) and DAPI (blue). **(C, D)** HEp-2 cells were incubated in Gln-free DMEM supplemented with ASNase or Asn (0.34mM) for 24 h, followed by immunostaining for CTPS (green) and DAPI (blue). **(E,**

F) HeLa cells were incubated with Gln-free DMEM supplemented with ASNase or Asn (0.34mM) for 24 h, followed by immunostaining against CTPS (green) and DAPI (blue). **(G)** HEp-2 cells were incubated in indicated conditions for 24 h, harvested and lysed for Western blotting analysis. Scale bars: 10 mm.

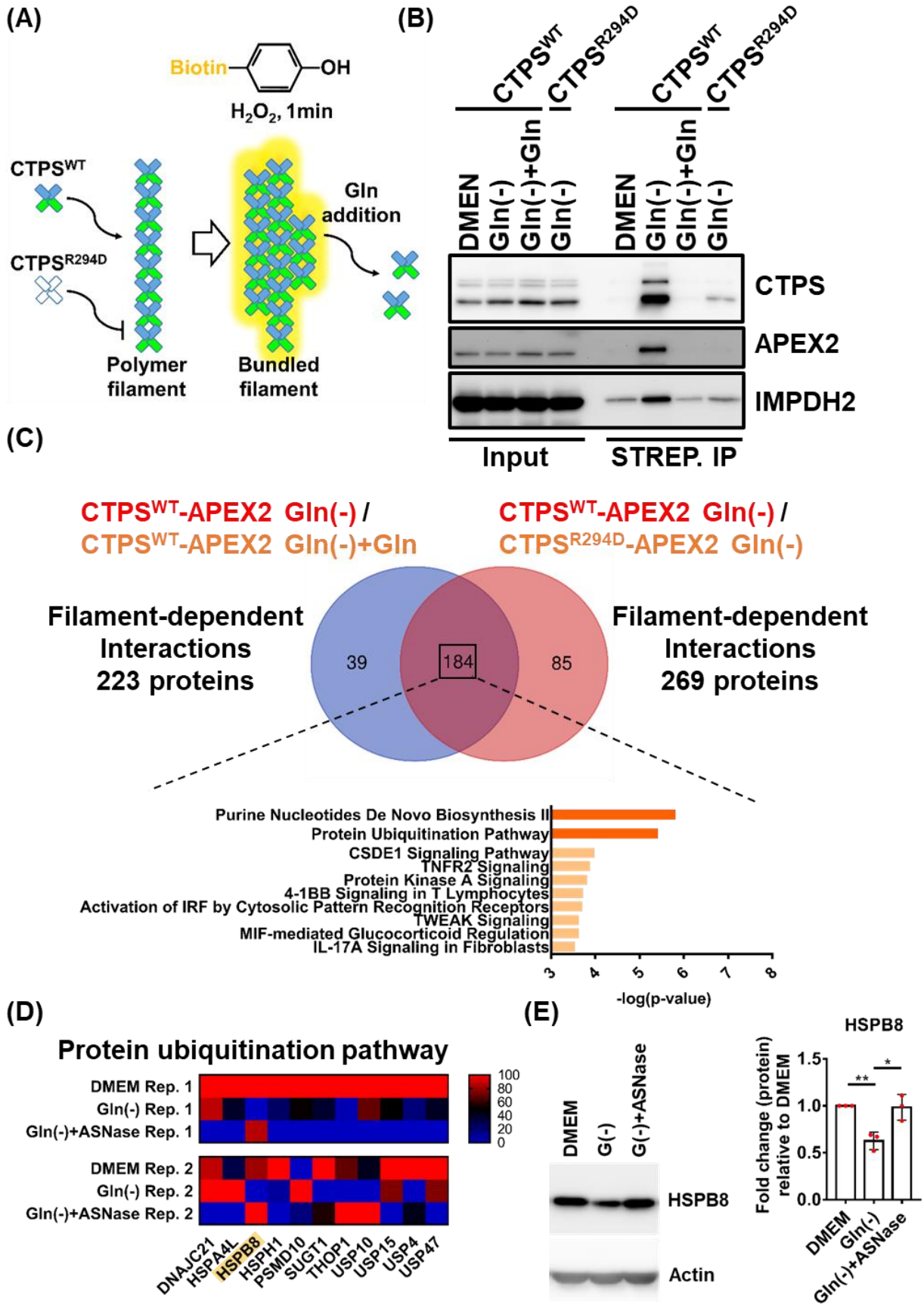

Figure 3. Proximity labeling identifies the protein quality control factor HSPB8 as a condition-specific interactor of CTPS

(A) Schematic of the CTPS-APEX2 proximity labeling strategy. **(B)** HEp-2 cells expressing CTPS^{WT}-APEX2 were cultured in DMEM, Gln-free DMEM, or Gln-free DMEM supplemented

with Gln for 24 h. HEp-2 cells expressing CTPS^{R294D}-APEX2 were cultured in Gln-free DMEM for 24 h. Biotinylated proteins were affinity purified using streptavidin-conjugated magnetic beads and analyzed by Western blotting. **(C)** Venn diagram showing 184 proteins common to the comparisons of CTPS^{WT}-APEX2 cells cultured in Gln-free DMEM versus Gln-free DMEM supplemented with Gln, and CTPS^{WT}-APEX2 versus CTPS^{R294D}-APEX2 cells cultured in Gln-free DMEM. Enriched pathways associated with CTPS-interacting proteins under Gln deprivation were identified by Ingenuity Pathway Analysis (IPA). **(D)** Heatmap showing proteins involved in the unbiquitination pathway in cells cultured in DMEM, Gln-free DMEM, or Gln-free DMEM supplemented with ASNase. **(E)** HSPB8 protein levels in cells cultured in DMEM, Gln-free DMEM, or Gln-free DMEM supplemented with ASNase.

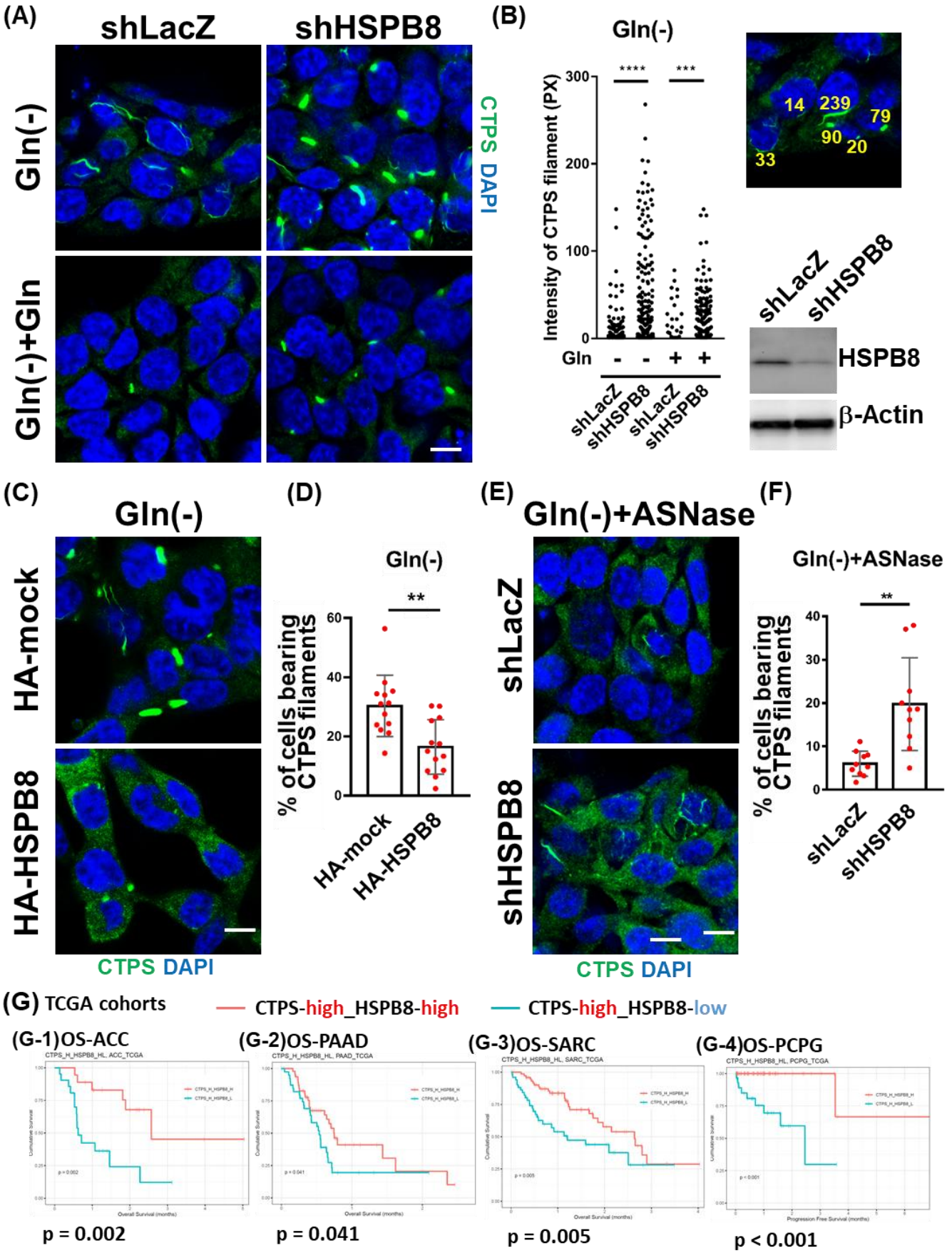

Figure 4. HSPB8 is required for the disassembly of CTPS filaments during nutrient stress

(A and B) HCT116 cells expressing shLacZ or shHSPB8 were cultured in glutamine-free DMEM for 24 h, with glutamine added for the final 30 min where indicated. Cells were

immunostained for CTPS (green) and DAPI (blue). CTPS filament intensity was quantified using ImageJ, with representative filament lengths indicated by pixel values (yellow). HSPB8 protein levels were assessed by Western blotting.

(C and D) HCT116 cells transfected with HA-mock or HA-HSPB8 were cultured in glutamine-free DMEM for 24 h and immunostained for CTPS (green) and DAPI (blue).

(E and F) shLacZ- and shHSPB8-expressing HCT116 cells were cultured in glutamine-free DMEM supplemented with asparaginase (ASNase) for 24 h and immunostained for CTPS (green) and DAPI (blue).

Scale bars, 10 μm.

(G) Kaplan–Meier overall survival analysis indicating that tumors with high CTPS and low HSPB8 expression (cyan) are associated with significantly reduced survival, compared to that with high CTPS and high HSPB8 expression (red), in adrenocortical carcinoma (ACC; G-1), pancreatic adenocarcinoma (PAAD; G-2), sarcoma (SARC; G-3), and pheochromocytoma and paraganglioma (PCPG; G-4).

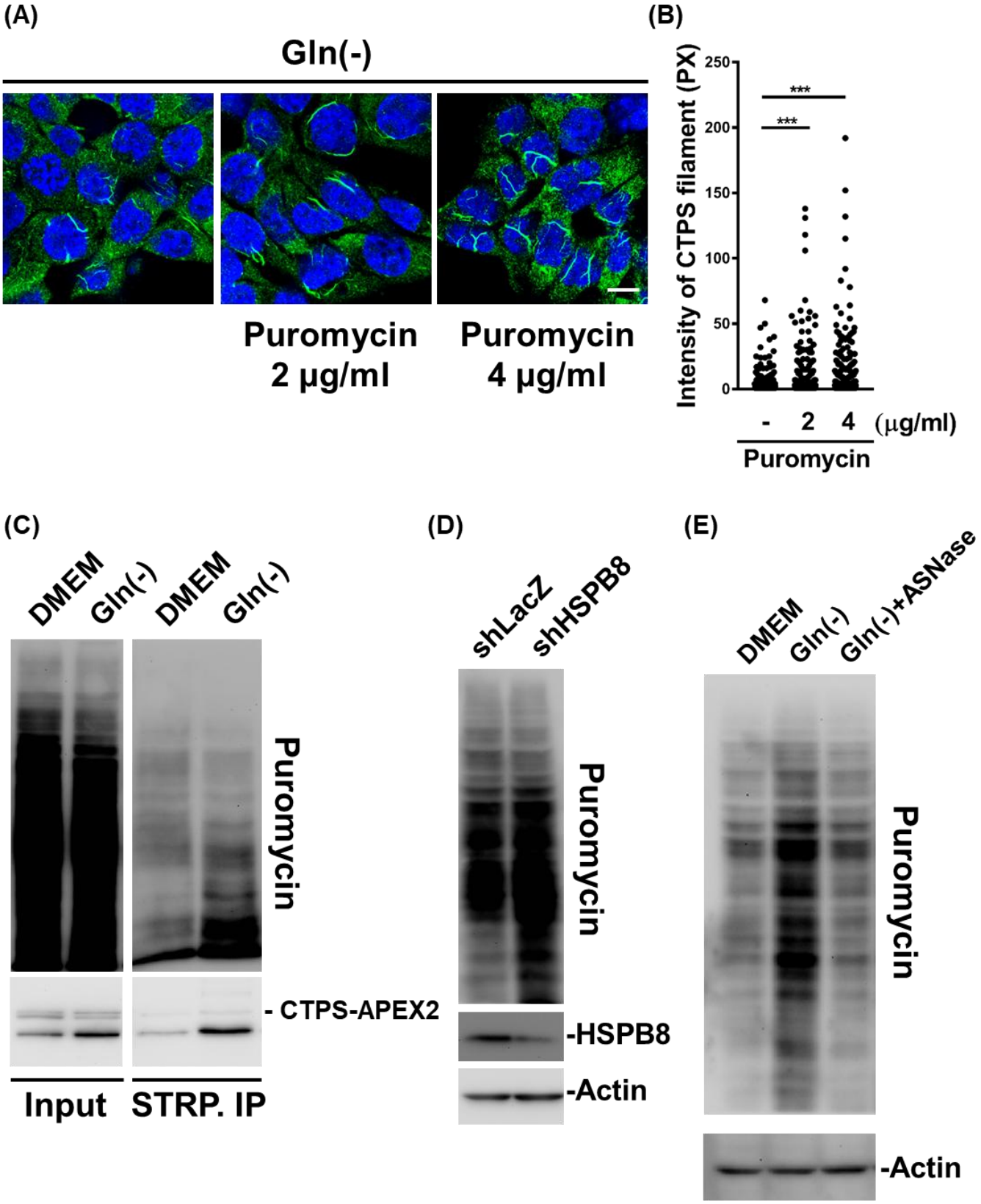

Figure 5. HSPB8-mediated protein quality control is associated with CTPS filament formation

(A and B) HCT116 cells were cultured in Gln-free DMEM for 24 h, with puromycin added during the final 3 h, followed by immunostaining for CTPS (green) and DAPI (blue). CTPS filament intensity was quantified using ImageJ.

(C) HCT116 cells expressing CTPS^{WT}-APEX2 were cultured in Gln-free DMEM for 24 h, with puromycin (10 μg/ml) added during the final 3 h. Proximity labeling was performed, and

biotinylated proteins were analyzed by Western blotting.
(D) shLacZ- and shHSPB8-expressing HEp-2 cells and **(E)** HEp-2 cells were cultured in Gln-free DMEM for 24 h, with puromycin (20 μg/ml) added during the final 10 min. Cells were harvested and analyzed by Western blotting for puromycin incorporation, HSPB8, and actin. Scale bars, 10 μm.

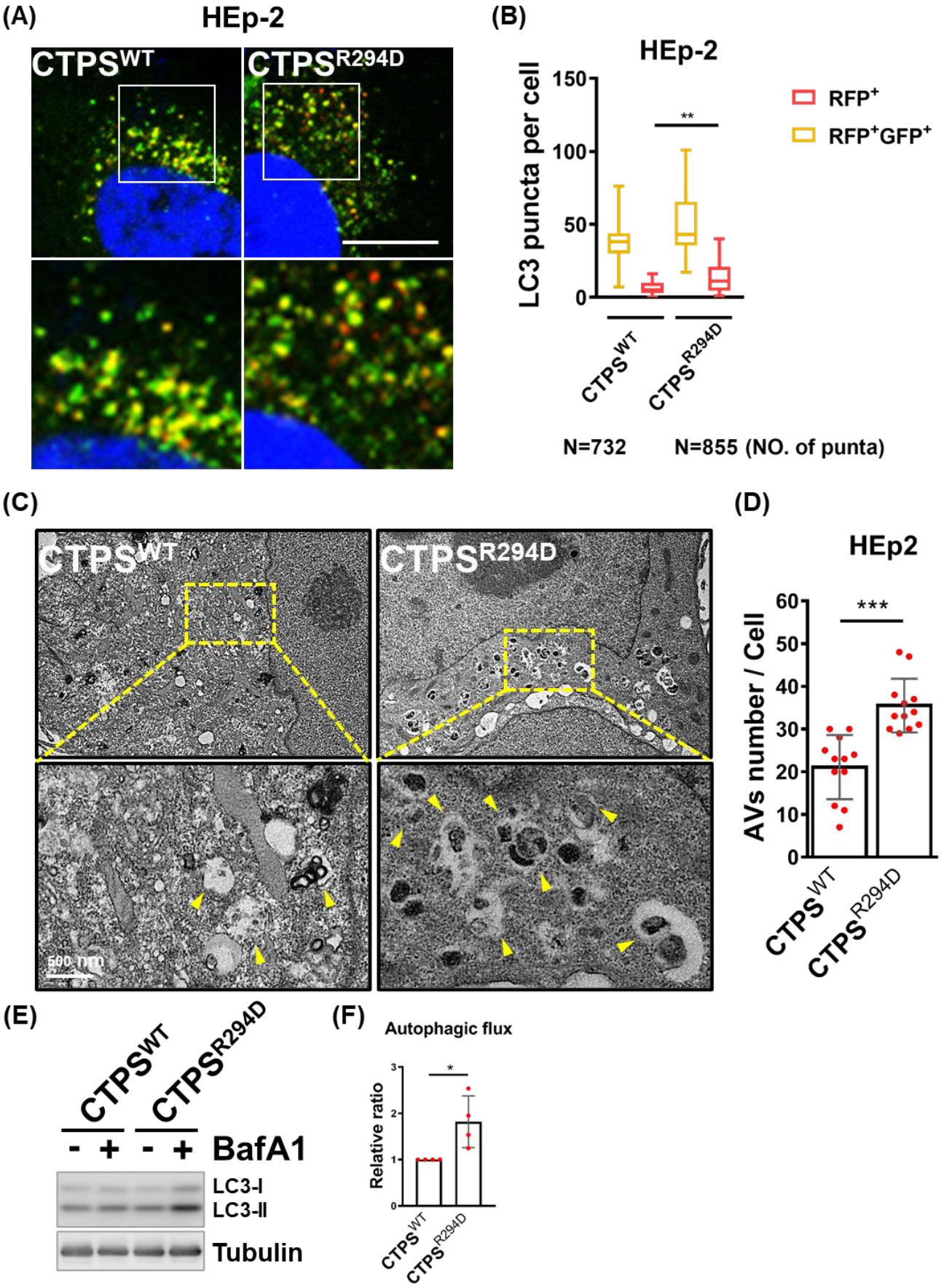

Figure 6. CTPS filament modulates autophagic flux under glutamine deprivation

(A and B) HEp-2 cells stably expressing $CTPS^{WT}$ or $CTPS^{R294D}$ and the tandem GFP–RFP–LC3 reporter were cultured in Gln-free DMEM for 24 h. GFP- and RFP-positive puncta were quantified using ImageJ.

(C and D) Transmission electron microscopy images of $CTPS^{WT}$ and $CTPS^{R294D}$ HEp-2 cells cultured in Gln-free DMEM for 24 h. Autophagic vesicles are indicated by yellow arrowheads. **(E and F)** Quantification of LC3-II levels in $CTPS^{WT}$ and $CTPS^{R294D}$ HEp-2 cells cultured in Gln-free DMEM for 24 h, with or without bafilomycin A1 (BafA1; 100 nM) added during the final 16 h.

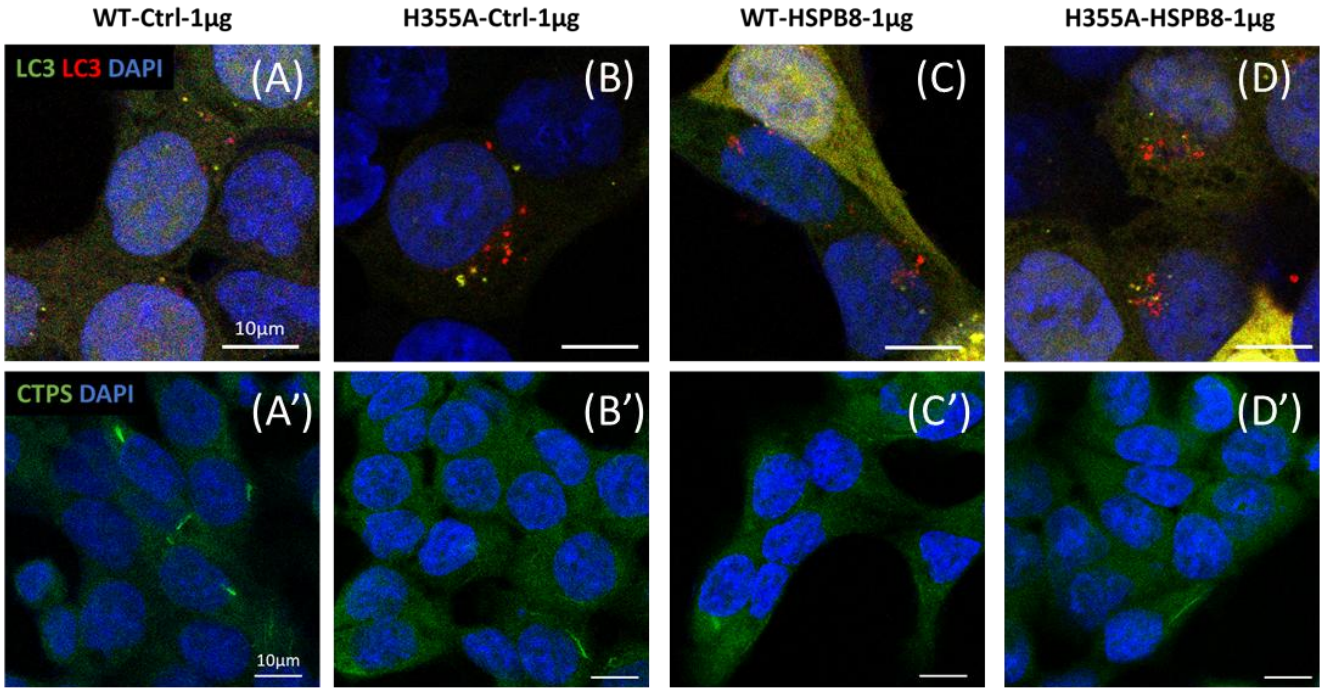

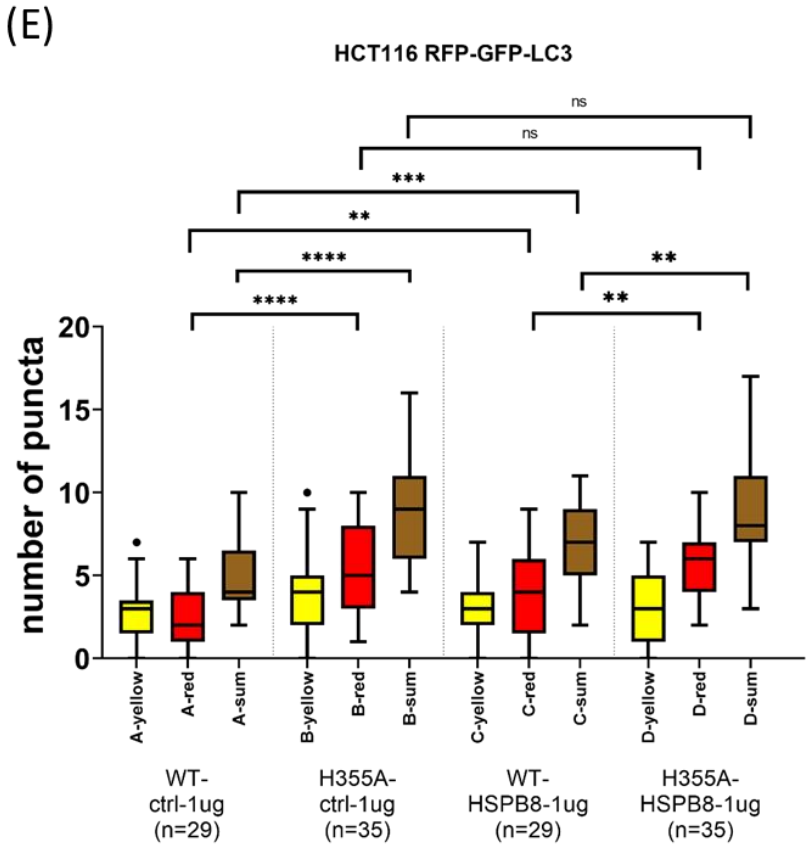

Figure 7. HSPB8 overexpression enhances autophagy inversely correlated with CTPS filament formation

(A–D) Representative images of autophagic vesicles in HCT116 cells expressing the tandem RFP–GFP–LC3 reporter. Red-only puncta indicate autolysosomes, while yellow puncta (RFP/GFP colocalized) mark autophagic structures; nuclei were counterstained with DAPI (blue).

(A′–D′) Corresponding images showing CTPS filament formation by immunostaining for CTPS (green) with DAPI (blue).

(E) Quantification of autophagic puncta per cell, including red-only, yellow, and total puncta. Numbers below each condition (n) indicate the number of cells analyzed per group. Scale bars, 10 μm.

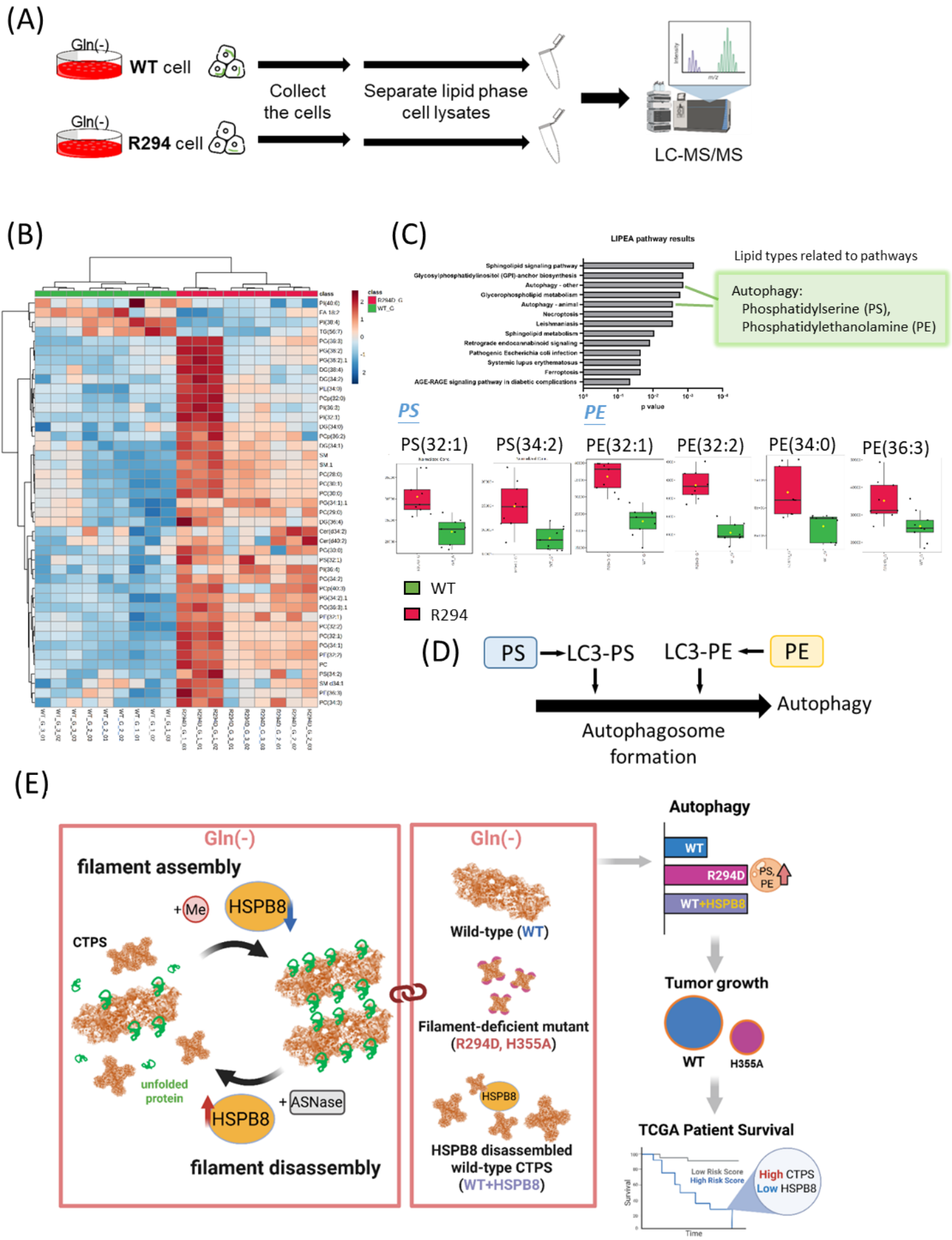

623 **Figure 8. Metabolomic profiling of phospholipids in cells expressing CTPS^{WT} versus**

filament-null CTPS mutant

(A) Scheme of the experiment design. HEp-2 cells stably expressing $CTPS^{WT}$ and $CTPS^{H355A}$ were cultured in Gln-free DMEM for 24 h, and subjected to lipid extraction, followed by LC/MS-MS analysis. Three independent experiments were performed and included in the analysis. **(B)** Heatmap showing the relative abundance of 43 identified metabolites across conditions. **(C)** Pathway annotation analysis of the 43 identified metabolites using LIPEA. **(D)** Phosphatidylserine (PS) and Phosphatidylethanolamine (PE) contribution to autophagy pathway. **(E)** Schematic illustrating the HSPB8–CTPS axis reveals a metabolic vulnerability in glutamine-stressed tumors. CTPS filament dynamics is suggested as a metabolic switch. Accumulation of unfolded peptides promotes CTPS filament bundling, a process modulated by cellular methylation. Under glutamine deprivation, reduced HSPB8 levels lead to the accumulation of misfolded peptides, thereby facilitating CTPS filament assembly. In contrast, increased HSPB8 expression, induced by asparaginase (ASNase), promotes CTPS filament disassembly and enhances CTPS enzymatic activity. Elevated CTPS activity supports CTP-dependent phospholipid synthesis, including phosphatidylinositol (PI) and phosphatidylethanolamine (PE), thereby driving autophagosome expansion and suppressing tumor growth. This regulatory axis reveals a metabolic vulnerability in tumors characterized by high CTPS and low HSPB8 expression.

Abbreviations: Me, methylation; ASNase, asparaginase.